**Title**: The potential for gas-free measurements of absolute oxygen metabolism during both baseline and activation states in the human brain

**Authors:** Eulanca Y. Liu[a,b], Jia Guo[b], Aaron B. Simon[b], Frank Haist[c,d], David J. Dubowitz[b,e], and Richard B. Buxton[b,e]

[a] Neurosciences Graduate Program, Medical Scientist Training Program, University of California, San Diego, USA
[b] Center for Functional MRI, University of California, San Diego, USA
[c] Psychiatry, University of California, San Diego, USA
[d] Center for Human Development, University of California, San Diego, USA
[e] Radiology, University of California, San Diego, USA

**Running title:** Gas-free measurements of oxygen metabolism in the human brain

**Corresponding author:**
R.B. Buxton (rbuxton@ucsd.edu)
University of California, San Diego, 9500 Gilman Drive, MC 0677, La Jolla, CA 92093-0677, USA

**Synopsis:** We tested noninvasive methods to measure absolute oxygen metabolism ($CMRO_2$) in both baseline and activation states without the use of special gases: VSEAN to measure baseline $O_2$ extraction fraction (OEF), and FLAIR-GESSE to measure $R_2'$ to estimate the scaling parameter *M*. Primary findings were: $CMRO_2$ changes to visual stimulation derived from $R_2'$ were similar to estimates based on hypercapnia-derived *M*; OEF values were in good agreement with previous PET findings; and, variation of baseline $CBF/CMRO_2$ coupling across subjects does not follow activation coupling, suggesting different mechanisms may be involved. These results support the potential of gas-free methods for quantitative physiological measurements.

**Purpose:** To demonstrate the potential for two non-invasive techniques, VSEAN and FLAIR-GESSE, for absolute measurements of $CMRO_2$ during both baseline and activation states.

**Abstract**

Quantitative functional magnetic resonance imaging methods make it possible to measure cerebral oxygen metabolism ($CMRO_2$) in the human brain. Current methods require the subject to breathe special gas mixtures (hypercapnia and hyperoxia). We tested a noninvasive suite of methods to measure absolute $CMRO_2$ in both baseline and dynamic activation states without the use of special gases: arterial spin labeling (ASL) to measure baseline and activation cerebral blood flow (CBF), with concurrent measurement of the blood oxygenation level dependent (BOLD) signal as a dynamic change in tissue $R_2^*$; VSEAN to estimate baseline $O_2$ extraction fraction (OEF) from a measurement of venous blood $R_2$, which in combination with the baseline CBF measurement yields an estimate of baseline $CMRO_2$; and FLAIR-GESSE to measure tissue $R_2'$ to estimate the scaling parameter needed for calculating the change in

2

$CMRO_2$ in response to a stimulus with the calibrated BOLD method. Here we describe results for a study sample of 17 subjects (8 female, mean age=25.3 years, range 21-31 years). The primary findings were that OEF values measured with the VSEAN method were in good agreement with previous PET findings, while estimates of the dynamic change in $CMRO_2$ in response to a visual stimulus were in good agreement between the traditional hypercapnia calibration and calibration based on $R_2'$. These results support the potential of gas-free methods for quantitative physiological measurements.

**Key words:** functional MRI, blood oxygenation level dependent, cerebral blood volume, hypercapnia, post-stimulus undershoot, cerebral metabolism of oxygen

**Abbreviations:**

BOLD: Blood Oxygenation Level Dependent

ASL: Arterial spin labeling

PICORE: Proximal inversion with control of off-resonance effects

QUIPSS II: Quantitative imaging of perfusion using a single subtraction II

VSEAN: Velocity-Selective Excitation and Arterial Nulling

FLAIR-GESSE: FLuid Attenuated Inversion Recovery Gradient Echo Sampling of Spin Echo

## 1. Introduction

The blood-oxygenation-level dependent (BOLD) signal has been used extensively for mapping changes of neural activity noninvasively in the human brain. However, the physiological complexity of the BOLD signal makes interpretation of BOLD data challenging, particularly in studies of development and disease. Quantitative fMRI methods, designed to measure the two physiological variables underlying the BOLD response—cerebral blood flow (CBF) and the cerebral metabolic rate of oxygen ($CMRO_2$)—may paint a more complete picture of neural physiology than BOLD alone. $CMRO_2$ reflects the energy cost of neural activity and, when paired with CBF, may potentially provide information on the activity of specific neural populations (Buxton et al., 2014; Uhlirova et al., 2016b, 2016a). In addition, quantitative physiological measurements have the potential to expand clinical applications of fMRI, such as yielding fundamentally different conclusions about underlying physiology than possible with BOLD alone. The primary goal of technological development in this area is to measure both baseline values and activation changes in CBF and $CMRO_2$ using quantitative physiological units. Quantitative and noninvasive measurements of CBF using arterial spin labeling (ASL) methods are now well established (Alsop et al., 2015). ASL allows for quantitative measurement of CBF across multiple image slices within a few seconds, depending on the technique and imaging volume. Given this short acquisition time, serial ASL images acquired over several minutes can either be averaged together to improve signal-to-noise ratio for average CBF measurement, or used as a dynamic time series to study CBF fluctuations over time (Griffeth and Buxton, 2011; Liu et al., 2019; Perthen et al., 2008).

In contrast, measuring $CMRO_2$ is challenging with any technique (Buxton, 2010), and measuring baseline and dynamic change must be approached with two different classes of methods. The *fractional* change in $CMRO_2$ can be measured with a calibrated BOLD approach based on simultaneous dynamic measurements of ASL and BOLD signals (Davis et al., 1998).

4

This approach requires an additional calibration experiment to determine a scaling parameter $M$ in the model of the BOLD signal. $M$ depends on the amount of deoxyhemoglobin in the baseline state of the individual, and directly scales the BOLD signal measured for that individual for given changes in CBF and $CMRO_2$. With this measured value of $M$, the CBF and BOLD responses to neural activation are analyzed with the same model of the BOLD signal to estimate the fractional change in $CMRO_2$. In the classic calibrated-BOLD method, $M$ is calculated on a voxel-wise or region-of-interest (ROI) basis from measured CBF and BOLD responses to a hypercapnia challenge (Davis et al., 1998), with the assumption that the elevated $CO_2$ produces a change in CBF with no change in $CMRO_2$. *Baseline* $CMRO_2$ is approached by measuring the baseline oxygen extraction fraction (OEF), and several techniques have been proposed based on different ways in which the oxygenation of blood affects the MR signal. A current technique uses measurements of the BOLD response to breathing a gas with elevated $O_2$, in conjunction with the measurements of the response to $CO_2$ (Bulte et al., 2012; Gauthier and Hoge, 2013; Merola et al., 2018; Wise et al., 2013).

This need to make measurements while the subject breathes controlled gas mixtures in the multi-gas approach makes quantitative fMRI a complicated procedure that limits wider application beyond research settings. In addition, wearing gas masks or breathing higher concentrations of $CO_2$ and $O_2$ would not be possible in some patient populations. To eliminate this barrier to entry into clinical applications, and for more widespread application of quantitative fMRI methods in basic brain studies, we evaluated two methods for measuring baseline and activation changes in $CMRO_2$ that do not require the subject to breathe special gas mixtures. The calibration information to estimate $M$ is based on measurement of tissue $R_2'$, essentially the component of transverse magnetization relaxation that can be reversed with a spin echo. Recent theoretical work (Blockley et al., 2015; Blockley and Stone, 2016), based on earlier seminal work of Haacke and Yablonskiy (Yablonskiy, 1998; Yablonskiy and Haacke, 1994),

5

showed that $R_2'$, like $M$, essentially depends on the total deoxyhemoglobin content of tissue. In this study, $R_2'$ was measured with a modified FLuid Attenuated Inversion Recovery Gradient Echo Sampling of Spin Echo sequence (FLAIR-GESSE) method (Simon et al., 2016). The baseline $CMRO_2$ measurement was done with a technique called Velocity-Selective Excitation and Arterial Nulling (VSEAN) (Guo and Wong, 2012) that isolates the signal of local venous blood and measures its relaxation rate $R_2$. Because $R_2$ depends primarily on the $O_2$ saturation of hemoglobin, applying an appropriate calibration curve provides a measurement of the local $O_2$ extraction fraction (OEF), and together with a baseline CBF measurement from ASL provides a measurement of baseline $CMRO_2$. In this study, we evaluated the combination of these two gas-free techniques to make absolute baseline and activation $CMRO_2$ measurements as an initial step toward more widespread applications of quantitative fMRI methods.

## 2. Methods

### 2.1 Subjects

Twenty-one healthy adults were recruited for the study. Inspired and end-tidal $O_2$ and $CO_2$ were monitored for all subjects throughout the run. Two of the 21 subjects were eliminated from the analyses because inspired and end-tidal $O_2$ and $CO_2$ measurements revealed leaks in the tubing or non-rebreathing facemask. Two other subjects exhibited no BOLD or flow change to the visual stimulus administration, demonstrating that the visual cortex was not well targeted. Thus, the study sample included 17 subjects (8 female, mean age=25.3 years, range 21-31 years). The study was approved by the Human Research Protections Program of the University of California, San Diego; written informed consent was obtained from all subjects. Subjects were remunerated for their participation.

*2.2 Gas administration*

Subjects were equipped with a non-rebreathing facemask (Hans Rudolph, KS, USA). The inspiratory port of the mask was connected to a large gas-tight balloon (VacuMed, CA, USA), pre-filled with a pre-mixed hypercapnia gas mixture of 5% $CO_2$, 21% $O_2$, balance $N_2$ (Airgas-West, CA, USA). The tubing (VacuMed, CA, USA) was disconnected to allow the subject to breathe normal room air in the normocapnic condition. End-tidal and inspired $O_2$ and $CO_2$ were monitored using a Perkin Elmer 1100 medical gas spectrometer (Perkin Elmer, Waltham, MA).

*2.3 Imaging*

2.3.1 BOLD-ASL. A dual-echo gradient echo spiral PICORE QUIPSS II ASL acquisition (Wong et al., 1998) was used to acquire simultaneous BOLD and ASL dynamic images on a General Electric (GE) Discovery MR750 3.0T scanner. Seven axial slices (5 mm thick/1 mm gap) covering the occipital cortex, centered around the calcarine sulcus, were obtained with TR=2500ms, TI1=700ms, TI2=1750ms, TE=3.3/30ms, 90° flip angle, FOV 256 mm x 256 mm, and matrix 64x64. Field maps with the same slice prescription were acquired to correct distortions in the spiral acquisition due to magnetic field inhomogeneity (Noll et al., 2005). Physiological monitoring was performed throughout the scan session using a pulse oximeter for cardiac cycle monitoring and respiratory bellows for respiratory dynamics (GE MR750 built-in).

2.3.2 VSEAN. The baseline $CMRO_2$ measurement was done with Velocity-Selective Excitation and Arterial Nulling (VSEAN) (Guo and Wong, 2012) that isolates the signal of local venous blood and measures its relaxation rate $R_2$. Because $R_2$ depends primarily on the $O_2$ saturation of hemoglobin, this provides a measurement of the local $O_2$ extraction fraction (OEF). This method differentiates the signal of slowly moving blood from that of static tissue by velocity selective excitation, i.e., selectively generating signal only from slow moving spins in arterioles

7

and venules. An arterial-nulling preparation module isolates the venous blood signal, measured with multiple $T_2$-preparations of different effective TEs (eTEs) (Guo and Wong, 2012). The sole center slice of the BOLD-ASL prescription was used as the single 10mm VSEAN slab. Details of the acquisition are as follows:

*Arterial nulling*: A slab-selective inversion pulse (arterial inversion slab thickness = 150mm) inverted a bolus of arterial blood below the imaging plane, with an inversion/delay time TI=1150ms to allow the inverted bolus of arterial blood to arrive at the imaging plane at the null point of the arterial blood's longitudinal magnetization during image acquisition. The spins of the static tissue and venous blood in the imaging slice were unperturbed, giving a strong venous signal.

*Velocity-Selective Excitation (VSE) for flow signal separation*: Two VSE pulse modules (one BIR4-based pulse train with velocity-sensitive gradient pulses, the second built into the image acquisition using only velocity-sensitive gradient pulses) excited and separated slow moving spins without generating signal from static or extremely slow flowing spins.

*$T_2$ measurement and oxygenation estimation*: $T_2$ preparation module (eTEs of 25/50/75ms with incremental gaps between RF pulses, built into the first BIR-4 based VSE module) measured $T_2$. The $T_2$ values were translated to blood oxygen saturation of hemoglobin Y via a $T_2$-Y calibration curve. We used the calibration curve from Zhao and colleagues based on a bovine blood sample measured *in vitro* at 3 Tesla (Zhao et al., 2007), which used a similar $T_2$ measurement setup as in this study. The equation for the curve used in this analysis is $T_2^{-1}(s^{-1}) = 8.3 + 33.6 \cdot (1 - Y) + 71.9 \cdot (1 - Y)^2$ (Guo and Wong, 2012). The OEF was then taken as 1-Y, based on the assumptions that arterial hemoglobin was fully saturated with oxygen and dissolved $O_2$ was negligible compared to hemoglobin-bound $O_2$.

*Other pulse sequence parameters*: FOV = 256 mm x 256 mm, matrix = 64 x 64, single-slice spin echo with spatial-spectral excitation, two slice-selective hyperbolic secant refocusing

8

pulses, single-shot spiral readout, TR/TE=3s/28ms, $v_e$=2 cm/s in slice-selective direction, slice-selective post-saturation pulses, 81 acquisitions preceded by two dummy scans and including six "cos" modulated reference scans (Guo and Wong, 2012). The total scan time was 4:03.

2.3.3 FLAIR-GESSE. We measured $R_2'$ with a FLuid Attenuated Inversion Recovery Gradient Echo Sampling of Spin Echo (FLAIR-GESSE) (Simon et al., 2016) technique. FLAIR-GESSE measures a series of gradient echo samples around a spin echo following Yablonskiy and Haacke's GESSE method with two main modifications (Simon et al., 2016). First, a CSF-nulling FLAIR module is added to minimize CSF contamination of $R_2'$ measurements. Our previous work has found that CSF-nulling improves the stability of $R_2'$ measurements (Simon et al., 2016). Second, the two sides of the echo are sampled with two acquisitions; each has a different spin echo time so that the acquired data are at the same absolute time after excitation. This helps correct for problems with multiple $T_2$ values within a voxel. Since $R_2'$ is sensitive to large-scale field inhomogeneity in addition to sub-voxel inhomogeneity due to deoxyhemoglobin, field offsets are acquired using phase images from the FLAIR-GESSE acquisition that are then used to calculate the large-scale field inhomogeneity and remove their contribution to the $R_2'$ estimate (Dickson et al., 2010; Simon et al., 2016). The center of each slice from the BOLD-ASL prescription was used, though for FLAIR-GESSE the slices were 2 mm thick (to minimize the effect of through-plane field gradients), with a gap of 4 mm. The pulse sequence parameters included two pairs of GESSE image series, one as an early spin echo series (63.6 ms after excitation) and one as a late spin echo series (83.6 ms after excitation), collected separately. For each spin echo series, 64 samples of each decay curve were collected asymmetrically. CSF nulling was chosen for middle slices, with a TR of 3.5 s, inversion time TI of 1.16 s, matrix = 64 x 64, and FOV = 256 mm x 256 mm. Each image slice was acquired in ascending order with a

9

spacing of 110 ms. Each of the two spin echo series was 3:58 in duration. $R_2'$ was calculated by the method described in Simon et al., 2016.

      2.3.4 Calibration and reference scans. A cerebral spinal fluid (CSF) reference scan using a single-echo spiral EPI acquisition (TE = 3.3ms) was obtained for CBF quantification (Chalela et al., 2000; Liu et al., 2004; Perthen et al., 2008). A minimum contrast scan (eight-shot spiral acquisition, TE=11ms, TR=2000ms) was made to correct for transmit and receive coil inhomogeneities (Wang et al., 2005). These reference and calibration scans used the same prescription as the ASL acquisition. A high resolution $T_1$-weighted anatomical scan (FSPGR) was acquired for image registration and segmentation.

*2.4 Stimulus paradigm*

      The visual stimulus task used to elicit neural activity in the occipital lobe (V1) was a black and white flickering radial checkerboard (6 Hz light-dark reversal frequency) with contrast and luminance as described in previous work (Simon et al., 2016). The central region was maintained at iso-luminant gray with visual angle ~1.5°. The stimulus was presented using MATLAB (2014a, The MathWorks, MA, USA) with the Psychophysics Toolbox extensions (Brainard, 1997; Pelli, 1997). The subject viewed the stimulus, projected onto a screen, through a mirror set atop the head coil.

*2.5 Experimental setup*

      BOLD and ASL responses were measured during a baseline task and to a visual stimulus in normocapnia. A hypercapnia calibration measurement and separate VSEAN and FLAIR-GESSE acquisitions in normocapnia were performed with the baseline task. The baseline state for all acquisitions performed in this experiment was a 1-back task (Kirchner, 1958) projected on a cross at the center of the screen. Subjects fixated at this center cross and

performed the 1-back task that presented single digits sequentially at random in 1-second intervals. The subjects were instructed to press a button on a response box each time they observed a number repeated sequentially. As this served as the baseline state, the task was performed continuously throughout each acquisition, with the ON or OFF states representing the presence of a visual stimulus, which was the flickering checkerboard described above filling the visual field surrounding the center cross. Given the 11-minute duration of the BOLD/ASL acquisition, the 1-back task was chosen as the baseline rather than a resting state (visual fixation on a cross) to hold the subject's attention throughout the long scan.

The BOLD/ASL acquisition consisted of an 11-min run, starting at normoxia/normocapnia with 3 blocks of 30-sec OFF/30-sec ON visual localizer at the beginning to independently determine an activated visual region of interest (ROI). The following experimental stimuli consisted of 2 blocks of 1-min OFF/1-min ON visual stimulus. The final 4 minutes of the BOLD/ASL acquisition was the calibrated BOLD experiment with a 1-min baseline period at normoxia/normocapnia, then a 3-min block of 5% $CO_2$ administration (normoxia/hypercapnia). A schematic of the run is shown in Figure 1.

The FLAIR-GESSE and VSEAN acquisitions as described above were all acquired at the baseline state (1-back task with no visual stimulus). Calibration and reference scans were acquired pre- and post-experimental acquisitions.

*2.6 Data preprocessing*

2.6.1 Arterial Spin Labeling (ASL) images: Raw ASL images were first corrected for inhomogeneity in the magnetic field using the field map acquisition (Noll et al., 2005). The functional scan was motion corrected and registered to one image in the 11-minute run using AFNI software (Cox, 1996). The first four images of the run were discarded to allow the signal to reach steady state. Minimum contrast images were used to correct ASL data for coil sensitivity

11

inhomogeneity (Wang et al., 2005). Applying surround-subtraction to the raw first-echo ASL images produced CBF-weighted images with minimal contamination from BOLD (Liu and Wong, 2005), and these were converted to physiological units (ml/100ml/min) using CSF as a reference (Chalela et al., 2000). A gray matter mask was determined from the absolute CBF, in which all voxels with CBF value greater than twice the mean CBF, taken as the average across all voxels, were included as part of the GM mask for each subject. Thus, the masks are generated from the BOLD/ASL acquisition, circumventing the need for anatomical registration to the functional data that could potentially distort voxels and thus the measurements. Empirically, we have found this threshold to give a good correspondence with GM masks generated from $T_1$-weighted anatomical images when the separate acquisitions are registered. For the visual ROI determination in 2.6.3, the gray matter mask was limited to the posterior third of the brain via a binary wedge-shaped mask covering the posterior third.

2.6.2. BOLD $R_2$*-weighted images: BOLD $R_2$*-weighted images were calculated from surround averaging of the first and second echo ASL images (Liu and Wong, 2005) to enable calculation of $R_2$* for each time point as previously reported (Liu et al., 2019). For each time series, after ROI selection (Section 2.6.3), the mean $R_2$* was subtracted to form a time series $\Delta R_2$*(t), which removed systematic effects of drift that scale identically with both echoes; $\Delta R_2$* was then converted back to a $\delta$BOLD signal without the drift effects (Liu et al., 2019).

2.6.3 Regions of interest (ROIs): Visual ROIs were generated using the ASL and BOLD responses to the 3-min visual functional localizer exclusively, then limited to the center slice that was used for VSEAN. A general linear model approach, described by Perthen et al. (Perthen et al., 2008), was used for ROI selection. The pattern of the stimulus was convolved with a gamma density function to produce a stimulus regressor (Boynton et al., 1996). A constant and a linear term were used as nuisance regressors. A mask containing only gray matter voxels, as determined in 2.6.1, in the posterior third of the brain was used to further restrict the ROI

selection. Voxels exhibiting both CBF and BOLD activations were detected using an overall significance threshold of p=0.05 and minimum cluster size of 2. Thus, the final visual ROI for each subject consisted of a single mask of voxels exhibiting independent activation in both CBF and BOLD to the visual stimulus, restricted to gray matter in the posterior third of the brain.

2.6.4. Average CBF and BOLD changes to stimuli. Average CBF and $R_2$* from BOLD (Section 2.6.2) time courses for the ROI were calculated for each subject, producing one-dimensional BOLD and CBF time courses. The resulting time series were normalized to an average baseline value, defined as the mean of the 15 seconds of rest before the first normocapnia visual stimulus (at the 4-min mark), the 15 seconds of rest before the second normocapnia visual stimulus (at the 6-min mark), and the 15 seconds of rest before the $CO_2$ stimulus onset (at the 8-min mark). These normalized values were used for all subsequent analyses. To allow time for the subjects' inspired and end-tidal gas levels to stabilize and equilibrate, data from the first minute of the hypercapnia block were not used subsequently. To derive single estimates of CBF and BOLD responses for each subject, the two visual stimulus blocks were first averaged.

*2.7 Calibrated BOLD and FLAIR-GESSE analysis*

In the classic calibrated-BOLD method (Davis et al., 1998) to measure the fractional change in $CMRO_2$ with activation, the BOLD signal is modeled as:

$$\delta BOLD_{act} = M \cdot \left(1 - (1 + \delta CBF)^\alpha \left(\frac{1 + \delta CMRO_2}{1 + \delta CBF}\right)^\beta\right) \qquad [1]$$

where the prefix "$\delta$" indicates the change in the variable normalized to the baseline value. The scaling parameter *M* is approximately proportional to the total deoxyhemoglobin content of tissue, which could vary across brain regions and subjects. The parameters $\alpha$ and $\beta$ were originally introduced to describe specific physical effects related to the change in venous blood

13

volume and nonlinearities of the magnetic susceptibility effects, respectively (Davis et al., 1998).

However, that original derivation left out several factors affecting the BOLD signal, and later

modeling studies including these factors found that the mathematical form of Eq. [1] is still

accurate, but the parameters $\alpha$ and $\beta$ are now thought of more as fitting parameters rather than

reflecting their original physical meanings (Buxton, 2013; Gagnon et al., 2016, 2015; Griffeth

and Buxton, 2011; Merola et al., 2016). The standard approach to estimate $M$ is to measure

CBF and BOLD responses to hypercapnia, and analyze the data with Eq. [1] and the

assumptions: 1) there is no $CMRO_2$ change during hypercapnia; and 2) particular values of $\alpha$

and $\beta$, typically $\alpha=0.2$ and $\beta=1.3$ (Chen and Pike, 2009; Griffeth et al., 2013; Mark et al., 2011).

With these assumptions, the scaling factor $M$ is calculated from the hypercapnia data. The

activation data are then analyzed with the estimated value of $M$ and the same assumed values

for $\alpha$ and $\beta$ to estimate the fractional $CMRO_2$ change to the stimulus.

In the current study, we compared the classic hypercapnia estimate of $M$ with a

measurement of $R_2'$, approximately the difference in transverse relaxation rates measured in

gradient echo and spin echo experiments: $R_2' \cong R_2^* - R_2$. The parameter $R_2'$ is sensitive to

magnetic field inhomogeneities due to 1) deoxygenated blood vessels, proportional to voxel

baseline deoxyhemoglobin concentration, like $M$, and 2) large-scale inhomogeneities of the

head. The inhomogeneity correction was done as in Simon et al., 2016, and the remaining $R_2'$

value was interpreted as reflecting deoxygenated blood vessels. Neglecting some of the

complexities of tissue relaxation (see Discussion for applicability and limitations), we would

expect $M \cong M' = TE \bullet R_2'$ (Blockley et al., 2015).

FLAIR-GESSE data were analyzed per Simon, et al. 2016. The raw GESSE data were

first averaged across the visual ROI before $R_2$ and $R_2'$ values were fitted to the averaged data.

Magnetic field inhomogeneities were corrected per Dickson et al. (Dickson et al., 2010). $M'$ was

calculated from $R_2'$ values through $M' \cong TE \bullet R_2'$. Fractional change in $CMRO_2$ ($\delta CMRO_2$) to the visual stimulus for each individual was calculated per Eq. [1] ($\alpha=0.2$, $\beta=1.3$) using the individual $M'$ value for each subject, as well as with the group mean $M'$, to compare estimates of $\delta CMRO_2$ using individual $M'$ versus group mean $M'$. Meanwhile, the hypercapnia response BOLD data were also substituted into Eq. [1] to yield an estimate of $M$ for each subject, calculated for $\alpha=0.2$, $\beta=1.3$. $\delta CMRO_2$ to the visual stimulus for each individual was then calculated per Eq. [1], ($\alpha=0.2$, $\beta=1.3$) using the individual $M$ value for each subject, as well as with the group mean $M$, to compare estimates of $\delta CMRO_2$ using individual $M$ versus group mean $M$. These values were compared to those using $M'$.

*2.8 VSEAN and baseline CMRO$_2$ analysis*

VSEAN data were analyzed per Guo and Wong (2012). Raw multi-echo data were averaged over the visual ROIs first, then used to fit a $T_2$ value representative of the entire ROI. The $T_2$ was then converted into blood oxygenation (Y) levels via $T_2$-Y calibration curve at 3T (Zhao et al., 2007). OEF was calculated from venous oxygenation (OEF = 1 – venous oxygenation). Baseline $CMRO_2$ was calculated from

$$CMRO_2 = CBF \cdot OEF \cdot CaO_2.$$ [2]

The equation to determine total arterial oxygen concentration is: $CaO_2$ = 1.36(Hb)($S_aO_2$/100) + 0.0031($P_aO_2$), with units as follows: $CaO_2$ in ml/dL, 1.36 ml $O_2$/1 g Hb, Hb in g/dL, $S_aO_2$ in %, 0.0031 g/dl/mmHg, and $P_aO_2$ in mmHg (Davenport, 1974). Hemoglobin concentration was assumed according to mean healthy ranges set by UC San Diego Health (Fraser and Haldeman-Englert, 2017); for females, [Hb] = 14g/dL; males, [Hb]=15.7g/dL. The age of each subject was also factored into $CaO_2$ determination through the estimate of $P_aO_2$ (Estimated normal $P_aO_2 \cong$ 100 mmHg – (0.3) age in years) (Crawford and Adesanya, 2010; Jurado and

Walker, 1969). CBF is expressed in ml/100ml/min, and $CaO_2$ from this equation is divided by 100 to give $CMRO_2$ units in ml/100ml/min. $CMRO_2$ in ml/100ml/min is then converted to mM/min (1 mL $O_2$ at 310 K, 1 atm = 0.03933 mmol $O_2$) (Davenport, 1974). For reference, 1 mM/min = 2.54 ml $O_2$/100 ml/min = 2.42 ml $O_2$/100g/min = 100 umol/100 ml/min = 95 umol/100g/min, with assumed density of blood = 1.05 g/mL at 310 K (Trudnowski and Rico, 1974).

*2.9 Voxel-wise analysis*

To compare the quality of VSEAN and FLAIR-GESSE data on a voxel-wise basis to ROI-based analyses, maps of OEF and $R_2'$ values were made for each voxel in the visual ROI. The masks were then further limited to encompass voxels that survived both to create dually-restricted (VSEAN and FLAIR-GESSE restricted) masks for the ROI. The median, mean, and standard deviation of the voxel-wise OEF and $R_2'$ estimates were calculated for each subject, then averaged across all 17 subjects.

*2.10 Data and code availability*

The data that support the findings of this study are available from the corresponding author, RBB, upon reasonable request. The data and code sharing adopted by the authors comply with requirements by the National Institutes of Health and the University of California, San Diego, and comply with institutional ethics approval.

## 3. Results

The following results present mean findings from the visual stimulus ROI (section 2.6.3). Voxelwise findings from the visual ROI and gray matter are described in the Supplementary

16

Materials. Those findings are not significantly different from the mean OEF and $R_2'$ calculated from the ROI-based method described here.

### 3.1 BOLD/ASL results

Average CBF and BOLD $R_2^*$ curves from 17 subjects across the entire 11-min acquisition are plotted in Figure 2. The average fractional change in CBF and BOLD to the visual stimulus and $CO_2$ challenge for each subject are plotted in Figure 2A. The average responses of the cohort are summarized in Figure 2B.

### 3.2 VSEAN results

Figure 3 shows the OEF measurements made using VSEAN within the visual ROI plotted against the baseline CBF (Fig. 3A), absolute $\Delta CBF$ to $CO_2$ (Fig. 3B), and absolute $\Delta CBF$ to visual activation (Fig. 3C). Pearson correlation analyses found no significant association with baseline OEF in any of these conditions (Baseline CBF: $r = -.188$, $p=0.470$, Cohen's $d=0.38$; Absolute $\Delta CBF$ to $CO_2$: $r = -.248$, $p=0.336$, $d=0.51$; $\Delta CBF$ to visual activation: $r = -.054$, $p=0.837$, $d=0.11$). The findings in Figs. 3A-C suggest possible sex differences in the CBF measures. Figure 3D summarizes OEF and CBF values of the entire sample, and separately for males and females. A two-way repeated-measures ANOVA revealed a significant main effect of sex ($F_{1,15}=7.103$, $p=.018$, $d=1.38$) with no significant sex by measure interaction ($F_{3,45}=2.096$, $p=.114$, $d=0.75$). Post-hoc analyses showed females had greater baseline CBF and absolute $\Delta CBF$ to $CO_2$ than males ($t_{15} = 3.090$ & $2.843$, Bonferonni corrected $p = .028$ & $.048$, $d = 1.51$ & $1.35$, respectively). No significant sex differences were detected in OEF or absolute $\Delta CBF$ to visual activation ($ts < 0.25$, $ps > .810$, $ds < 0.12$). Similar effects have been reported previously in work studying regional differences in CBF by sex (Esposito et al., 1996; Gur and Gur, 1990; Rodriguez et al., 1988).

17

*3.3 FLAIR-GESSE and M calibration results*

Mean measured $R_2'$ across 17 subjects in the visual ROI was 3.60 s$^{-1}$, with a standard deviation of 1.39 s$^{-1}$, giving a mean value of *M'*=0.108 +/- 0.04 (Figure 4B). The calibrated BOLD analysis of the hypercapnia data yielded an average estimate of *M* = 0.095 +/- 0.05 (Figure 4B). Figure 4A shows a plot of the individual data for *M'* against the value of *M* calculated for $\alpha$=0.2 and $\beta$=1.3. We also compared *M* and *M'* with OEF for each subject and found no statistically significant correlation (see Supplementary Materials for details). $\delta CMRO_2$ calculated using individual and group mean *M* and *M'* are reported in Figure 4C. While individual and group mean *M'* values yielded similar $\delta CMRO_2$, individual *M* from hypercapnia yielded significantly smaller mean $\delta CMRO_2$ than that of the group mean (p=0.049).

*3.4 Absolute CMRO$_2$ and CBF measurements*

The measured data provided the essential information needed to make estimates of absolute CBF and $CMRO_2$ in the baseline state and absolute change in CBF and $CMRO_2$ to the visual stimulus, thus yielding a complete quantitative picture of underlying physiology. These relationships are shown in Figure 5. The average baseline $CMRO_2$, determined using Eq. [2] and OEF=0.44 from VSEAN, was calculated to be 2.58 +/- 0.53 mM/min, equivalent to approximately 6.56 ml/100ml/min = 6.24 ml/100g/min = 258 umol/100ml/min = 245.1 $\mu$mol/100g/min (see section 2.8 for conversion). The table in Figure 5E shows the mean measured absolute change in $CMRO_2$ to the stimulus using *M'* values for each subject calculated from $R_2'$, based on $\alpha$=0.2 and $\beta$=1.3. Because this estimate depends on the estimate of the fractional $CMRO_2$ change, it also depends on the assumed value of $\beta$. The absolute $\Delta CMRO_2$ to a visual stimulus was estimated to be 0.21 mM/min for $\beta$=1.3. Figure 5 shows the

18

spread of individual measurements for these parameters. Importantly, in Figures 5A and 5B, the $x$ and $y$ axes are not independent measures as the value of baseline $CMRO_2$ was calculated from baseline CBF.


## 4. Discussion

This work explored the feasibility of making absolute measurements of $CMRO_2$ and CBF without requiring the subject to breathe special gases as a first step toward more widespread application of quantitative physiological measurements. While arterial spin labeling (ASL) techniques that do not involve gases are well developed to measure both baseline and fractional change in CBF, $CMRO_2$ measurement is much more challenging and often involves administration of gases with higher concentrations of $O_2$ or $CO_2$. The main barrier to measuring baseline $CMRO_2$ is obtaining a measurement of oxygen extraction fraction (OEF), while measuring fractional change in $CMRO_2$ to a stimulus requires calibration of the blood oxygenation level dependent (BOLD) signal through the factor $M$.

The two gas-free techniques tested here present ways to measure those parameters noninvasively. Velocity-selective excitation and arterial nulling (VSEAN) is a technique that leverages relaxation effects of altered hemoglobin $O_2$-saturation on the transverse relaxation rate ($R_2$) of venous blood to determine regional OEF. Fluid attenuated inversion recovery – gradient echo sampling of spin echo (FLAIR-GESSE) is a method of estimating the factor $M$ through measurement of $R_2'$ that reflects the amount of total deoxyhemoglobin in tissue. We applied these methods to a relatively homogeneous cohort of 17 subjects. Because of the uniformity of the study population, we expected that the physiological parameters were likely to be similar across subjects, and that the variance of the measured values across subjects was thus likely to be dominated by the intrinsic variability of the measurement methods. We took this conservative approach in interpreting the performance of these methods. Our primary findings

19

were: 1) VSEAN yielded a mean value of baseline OEF in the visual ROI of $0.44 \pm 0.08$, matching previously reported measurements of extraction (Ibaraki et al., 2007; Ishii et al., 1996; Ito et al., 2004) using positron-emission tomography (PET); and 2) the estimated changes in $CMRO_2$ in response to the visual stimulus were similar when calculated from *M'*, which was estimated from $R_2'$ measured with the FLAIR-GESSE method, and when calculated from *M* estimated from the hypercapnia response. The ability to obtain a complete quantitative picture of human brain activation, with absolute measures of CBF and $CMRO_2$ in both baseline and activation states, would be a useful tool for basic studies of brain function and for clinical applications to characterize the effects of disease.

### 4.1 Baseline $CMRO_2$ with VSEAN OEF measurement

The VSEAN method is an extension of the seminal method QUIXOTIC for measuring baseline OEF (Bolar et al., 2011), expanding on the basic idea to overcome some limitations of the earlier technique. QUIXOTIC uses a velocity-selective (VS) spin labeling technique, separating venous blood from arterial blood and static tissue. However, the sequence design causes the venous signal to be potentially contaminated by signal contribution from CSF due to diffusion attenuation and to be attenuated by a global inversion pulse. VSEAN addresses these issues by isolating the venous blood signal using a separate arterial nulling module and improves upon the signal to noise of measuring venous $T_2$ by selective excitation of moving venous spins right before acquisition which allows more time for venous spins to recover, thus yielding a stronger venous signal in comparison to that of QUIXOTIC, where a global inversion pulse attenuates all signal, including venous signal.

Although VSEAN had limited testing in human subjects previously, this is the first study utilizing VSEAN on a larger sample of subjects as part of a complete physiological

measurement. The accuracy of the measured mean OEF value over multiple subjects demonstrates its utility as a non-invasive method of estimating baseline $CMRO_2$. Mean OEF value across 17 subjects in visual ROI was 0.443 +/- 0.08. These are similar to previously reported OEF values determined using PET. Ishii et al. reported OEF=0.413 +/- 6.1 in the visual cortex; Ibaraki et al. reported 0.39 +/- 0.05 in occipital cortex (Ibaraki et al., 2007; Ishii et al., 1996). The absolute baseline $CMRO_2$ calculations were 2.58 +/- 0.53 mM/min (approximately 6.56 ml/100 ml/min) for visual ROI. This is higher than previously reported PET values for baseline $CMRO_2$; Ishii et al. reported 4.36 +/- 1.03 ml/100ml/min in visual cortex, while Ibaraki et al. reported 4.3 +/- 0.7 ml/100ml/min in occipital cortex (Ibaraki et al., 2007; Ishii et al., 1996). Part of this difference is most likely due to a higher baseline CBF in our study due to the active baseline. There are multiple components to the active baseline—a visual component, as the subject is fixating on the changing numbers, an attention/memory component, as the subject is focused on the order of the numbers, and a motor component in the form of button presses. As a result, the higher CBF baseline is likely due to the involvement of the task, as compared to a resting baseline with the subject simply lying still. Baseline CBF was determined to be 72.7 +/- 11.8 ml/100ml/min in visual ROI. This is compared to 66.1 +/- 12.9 in visual cortex (Ishii et al., 1996), or 58 +/- 11 ml/100ml/min in occipital cortex (Ibaraki et al., 2007), as reported previously. In addition, we observed a striking difference in the CBF between our female and male subjects, and considering the large effect size equaling 1.5 standard deviations, we feel confident in concluding that female CBF is greater than male CBF overall. While a difference in hematocrit between males and females could affect blood $T_2$* and thus produce an artefactual difference in the ASL measurements, the data here were collected with a short echo time that minimized such an effect (< 2%).

Interestingly, the correlation between baseline OEF and baseline CBF was weak (i.e., small effect) and nonsignificant. It is possible that a baseline OEF around 40% is in some sense

21

optimal, and that across subjects, baseline CBF adjusts to produce this OEF for the $CMRO_2$ demands of the individual. The distribution of OEF measurement across the group was thus much tighter than CBF measurements, which has been documented previously using other techniques (He and Yablonskiy, 2007; Raichle et al., 2001). Additionally, the variance observed is reflective of the variance in measurement technique combined with true variance across subjects. Because of the uniformity of the subject population, we did not expect large physiological variations in OEF across the subject pool. We thus could assume that the variance observed is dominated by the variance in measurement technique. The variance across subjects in measuring OEF with VSEAN compared to the variance using PET measurements was similar, or even better, depending on the study, as noted above. VSEAN could thus be a comparable technique to utilize that does not require the invasiveness of PET.

At this point, further development of these techniques will allow clinical researchers to assess how regional metabolism is altered in disease states. VSEAN would be a useful tool in using group mean results to determine changes in $CMRO_2$ in pathophysiology. Studies of human development, healthy aging, and disease would benefit from being able to assess group differences in baseline $CMRO_2$. There are limitations, however, to the types of diseases to which the methods could be applied; underlying changes to blood flow, blood content, and vasculature in some medical conditions could violate certain assumptions of the acquisition techniques. The pathophysiology of each disease process should be considered in the interpretation of these measurements, and more work is needed to understand how to best apply these methods in clinical applications. A subsequent paper will address the utility of individual and group OEF measurements in detecting $CMRO_2$ change in a single subject after significant alteration with drug administration.

Potential limitations of VSEAN include (1) low signal-to-noise (SNR) in certain voxels and (2) measurements that rely on a calibration curve developed using *ex vivo* bovine blood.

22

With regard to (1) low SNR, multi-echo spin echo measurements allow for higher temporal resolution and efficiency, but the accuracy of the $T_2$ measurement may be affected by flow artifacts through the multi-echo gradients echo-refocusing effects, and wash-out effects (Guo and Wong, 2012). To combat this, OEF is not calculated on a voxel-wise basis, and instead a $T_2$ fit is calculated for the average signals for each echo across a pre-defined mask. To address (2) the use of an *ex vivo* bovine blood calibration curve, while a $T_2$-Y calibration curve has been published using human blood samples by Lu and colleagues (Lu et al., 2012), this curve was not used due to a different $T_2$-preparation module (hard composite pulses vs. BIR-4 based), a different way of modulating eTEs (increasing the number of pulse modules vs. increasing the gap in the module), and its limited range. The authors noted that the relevant oxygenation range for venous blood, 0.5-0.75, was not tested (Lu et al., 2012); since VSEAN was developed specifically to measure blood oxygenation at those lower levels, the calibration curve using human blood was forgone for the Zhao curve that has a range of 0.39-1.00 for Hct=0.44. We would, however, still expect an effect of hematocrit on $T_2$ values as shown by previous investigators (Golay et al., 2001; Lu et al., 2012), and thus the estimate would most benefit from a Y-Hct dependent calibration curve, were it available, to control for the effect of hematocrit.

*4.2 ΔCMRO$_2$ from FLAIR-GESSE R$_2$′-M calibration*

Like VSEAN, previous studies have not evaluated FLAIR-GESSE to quantify CMRO$_2$ in a large sample of subjects. Here, we assumed the ideal relationship $M' \cong TE \bullet R_2'$ to calculate $M'$ values that we then used to calculate $\delta$CMRO$_2$ to a stimulus. An interesting aspect of our findings is the apparent difference in the relationship of baseline CBF to CMRO$_2$ versus in response to visual activation (Figs. 5A and 5B). We did not find a significant relationship between CBF and CMRO$_2$ in the baseline condition (Fig. 5A); however, the medium effect size

23

of the relationship (Cohen's $d$ = 0.97) suggests it would achieve significance with a slightly larger sample. In contrast, there was no ambiguity in the strength of the positive relationship between CBF and $CMRO_2$ in response to visual activation (Fig. 5B), which was a very large and significant effect ($d$ = 5.23). Overall, our results provide clear evidence for a physiologic difference in the coupling of flow and metabolism at baseline versus with activity. At baseline, the coupling is modest, whereas there is tight coupling during activation.

Empirically, our group estimate of $M'$ closely resembled the $M$ calculated from a hypercapnia experiment, with $\alpha$=0.2 and $\beta$=1.3. However, both $M$ and $M'$ depend on assumptions employed in the modeling that complicate direct physiological interpretation of these parameters (Simon et al., 2016). The value of $M$ estimated from a hypercapnia experiment depends on the version of the BOLD model used for the analysis, specifically the assumption of values for $\alpha$ and $\beta$, and also the assumption that there is no $CMRO_2$ change with hypercapnia. For the newer method, the estimate of $R_2'$ may depend on the acquisition technique and analysis, because the signal decay described by $R_2'$ is not a simple mono-exponential decay. Furthermore, theoretical modeling suggests that $M$ is expected to be larger than $M'$ due to diffusion and other BOLD effects associated with activation that are not captured by baseline $R_2'$, such as blood volume changes or intravascular signal changes (Blockley et al., 2015).  In practice, uncorrected field distortions, particularly near the edges of the brain where field distortions are likely to be the most nonlinear (Dickson et al., 2010), would tend to make larger estimates of $R_2'$ and thus $M'$. Additionally, different acquisitions have been shown to yield different values of $R_2'$; work by Ni and colleagues showed GESSE returned lower GM $R_2'$ measurements than asymmetric spin echo (ASE) and lower WM $R_2'$ than both ASE and gradient-echo sampling of free induction decay and echo (GESFIDE) (Ni et al., 2015). A scaling of $M'$ may be necessary depending on the acquisition method used. In short, whether one is

using $M'$ or $M$ to calibrate a BOLD/ASL experiment and measure $CMRO_2$, one needs to be mindful of the potential for systematic effects on accuracy due to the modeling assumptions and acquisition methods. The current results support the feasibility of doing a calibrated experiment without hypercapnia, but further work is needed to clarify the precise physical and physiologic effects underlying $M$ and $R_2'$ and their relationship.

As a test of the statistical properties of the standard hypercapnia method and the newer $R_2'$ method, we compared the distributions of $\delta CMRO_2$ values across the population estimated in two ways: first, using the individually measured values of $M$ or $M'$, and second, with the assumption that each subject's value of $M$ or $M'$ was the same and equal to the group mean value. The rationale for this comparison is that in general we expect that true variation of the physiological effects modeled by $M$ would lead to increased variance of the $\delta CMRO_2$ values estimated across a population, if not taken into account, and use of individual measurements of $M$ should then reduce the variance of $\delta CMRO_2$ compared to using a constant value of $M$ for all subjects. However, if there is significant random error in the measurement of $M$, and the true physiological range of the physiological parameters across the population is narrow, using individual $M$ values could increase the range of estimated $\delta CMRO_2$ across the population due to that random error. A conservative assumption is that the physiological factors that determine $M$ and $\delta CMRO_2$ to the stimulus are relatively uniform across our sample of young, healthy control subjects, and thus the observed variance of the estimates of $\delta CMRO_2$ across the population is likely a reflection of measurement error of $M$. The mean and standard deviation of the estimates of $\delta CMRO_2$ calculated using individual $M'$ values closely matched changes calculated using the group mean $M'$, consistent with this assumption and only a small role of random error of individual $M'$ estimates. However, for the hypercapnia data the same comparison showed that the distribution $\delta CMRO_2$ estimates from individual $M$ values had a mean reduced by more than

25

a factor of two, which may be due to the interaction of noisy signals with the nonlinearity of the calculation of $M$ using Eq [1]. In addition, the variance increased by about a factor of two compared with the $\delta CMRO_2$ distribution estimated from the group mean $M$, consistent with high variability of the individual $M$ measurements. It may be that the higher variance of $\delta CMRO_2$ estimates with individual $M$ values is due to our method of $CO_2$ administration, and it is possible that real-time end-tidal forcing could yield more consistent results on an individual basis. However, dedicated equipment to enable end-tidal forcing further restricts the application of quantitative physiology methods to dedicated research laboratories, supporting the push to work toward replacing gas-based techniques with gas-free based techniques.

Finally, it is important to note that $R_2'$ measurements, like the OEF measurements with VSEAN, may be most useful in fMRI studies of development, aging and disease in which different groups are compared. For example, a different mean $R_2'$ for children and adults in the brain region associated with performing a particular task could indicate that a difference in the BOLD response between the two groups should be interpreted with caution; the BOLD response difference may reflect a difference in baseline conditions rather than a difference in neural activity. Even if there is uncertainty about the exact relationship between $M$ and $M'$, as discussed above, simply normalizing the BOLD response by the mean $R_2'$ for the group would remove the baseline dependence, and any remaining difference between the two groups could be interpreted as due to differences in the $CMRO_2$ and CBF responses to the stimuli. If the CBF response also is measured, this will enable interpretation of whether the $CMRO_2$ response is different in the two groups based on the measured $R_2'$.

*4.3 Voxel-wise versus basic ROI-wise analyses*

Our primary analysis of the data focused on a functionally localized ROI in visual cortex. In this approach, all the raw data for voxels within the ROI were first pooled before calculating the physiological variables. That is, fractional CBF and BOLD responses were calculated after pooling the raw voxel data, and OEF and $R_2'$ were calculated after pooling the raw data for voxels within the ROI. This approach was used to provide a basic proof of concept of estimating absolute physiological parameters for both baseline and activation states. In principle, this approach could be extended to voxel-wise analysis, although this will require further developmental work. There are two central problems: 1) the VSEAN measurement suffers from poor estimation of $R_2$ when the signal to noise ratio is low; and 2) the $R_2'$ measurement is likely to be positively biased in regions where large-scale field correction is incomplete. For this reason, not every voxel in the visually activated ROI and GM masks may contain accurate information on OEF and $R_2'$. As a first step in beginning to extend these measurements to individual voxels, we chose limits on the quality of fit of $R_2$ in the VSEAN experiment and on the range of $R_2'$ as markers of data of sufficient quality to make an estimate of the associated parameter for that voxel. We then tested how many of the voxels chosen to be in the visual cortex ROI based on the activation data also had good quality estimates of OEF and $R_2'$. While a relatively large fraction of ROI voxels had a full set of measurements, there is clearly room for more work to improve the robustness of these measurements. Importantly, when we performed individual voxel analyses on just these voxels and then averaged over the calculated values, the basic physiological parameter estimates were similar to the ROI-approach of first pooling the data: the mean or median derived from voxel-wise analysis were not statistically different from the mean OEF and $R_2'$ derived using the basic visual ROI mask. In the future, simply using a

27

visual ROI determined from the functional localizer and GM mask from the ASL flow data may

be enough to make representative estimates of OEF and *M*.

## 4.4 Physiological results

The primary goal of this work was to begin to evaluate methods for making quantitative

physiological measurements without requiring the subject to breathe special gas mixtures. To

that end, a homogeneous group of young adult subjects was studied, and we did not expect

there to be large physiological variation across subjects. We found no statistically significant

correlations between baseline OEF and baseline CBF, nor between baseline OEF and *M* or *M′*.

For the latter, we expect *M* to scale with total deoxyhemoglobin in the baseline state, and total

deoxyhemoglobin should scale with the product of OEF and baseline venous blood volume. Part

of the variability of *M* may be due to variability of blood volume. Further work is needed to test

these methods in a wider range of subjects where more physiological variation could be

expected. Looking at sex differences in the measured physiological parameters, we found

baseline CBF to be significantly higher in females compared to males by about 22%. One of the

potential advantages of a fully quantitative assessment of CBF and $CMRO_2$ in both the baseline

and activation states is that we can examine absolute changes to a stimulus in addition to the

more commonly measured fractional changes. In comparing absolute baseline values of CBF

and $CMRO_2$ and absolute changes in these quantities to the stimulus, we found a different slope

(Figure 5A and 5B). This suggests that different physiological mechanisms may serve to

balance baseline CBF/$CMRO_2$ coupling and activation CBF/$CMRO_2$ coupling, although more

work is needed to define these mechanisms.

28

## 5. Conclusions

The results from this work demonstrate the potential for making absolute $CMRO_2$ measurements without requiring the subject to breathe special gases. However, work is still needed to refine these methods and establish their validity. Each method has its own challenges: for VSEAN, low SNR of the isolated blood signal for some voxels, and for FLAIR-GESSE, excessive field distortion near edges of the brain. Nevertheless, these results support the feasibility of painting a more complete picture of brain physiology, in absolute terms, during both baseline and activation states, with the potential of providing a deeper probe of neural activity in the human brain.
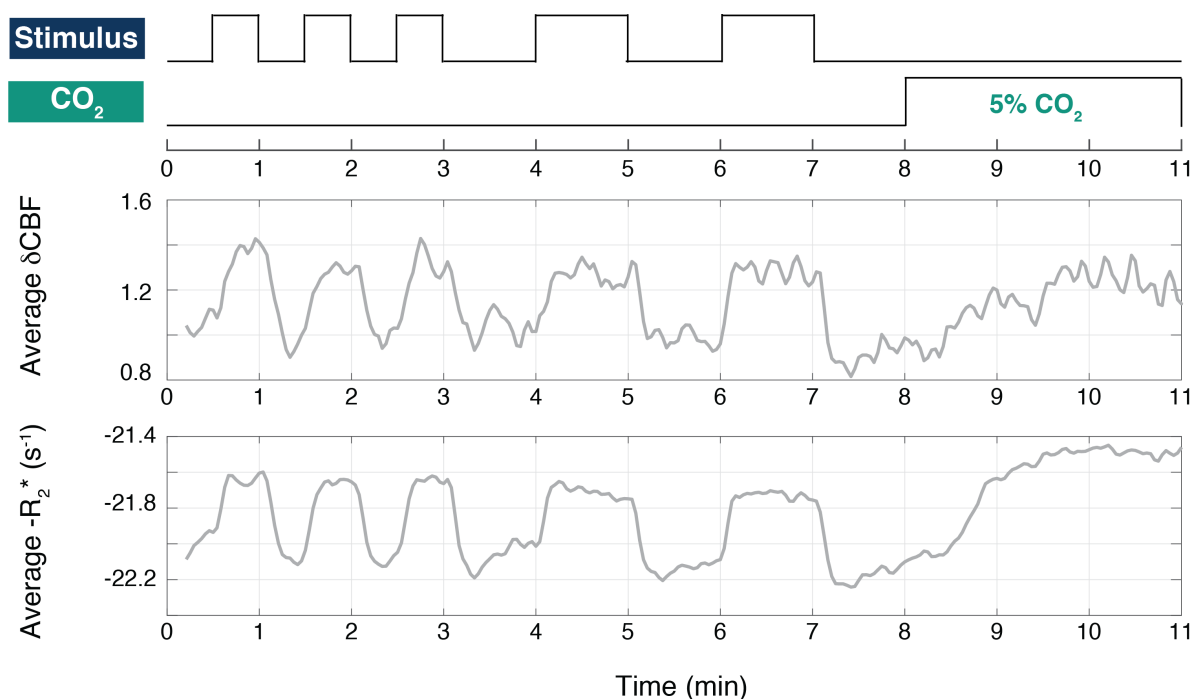
**Figure 1: Experimental set-up, CBF and R$_2$* data.** Top panel shows experimental set-up of PICORE QUIPSS II BOLD/ASL acquisition with visual stimuli of a 6 Hz flickering checkerboard ("Stimulus") and 5% $CO_2$ administration. Middle and bottom panels illustrate average CBF and BOLD R$_2$* curves across 17 subjects. The CBF is normalized to the baseline CBF, and thus is dimensionless. The BOLD R$_2$* curve is plotted as –R$_2$* for more visibly intuitive purposes.
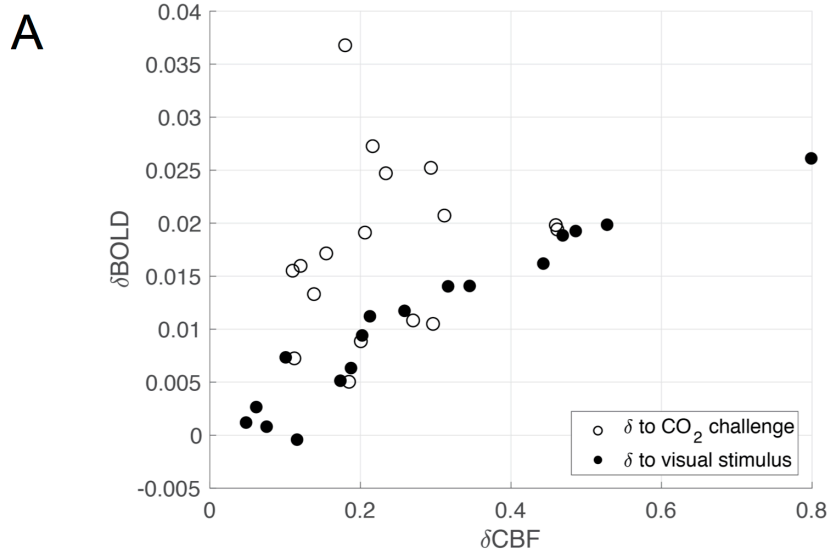
**Figure 2: Visual activation and calibrated BOLD results.** (A) Scatter plot of fractional CBF versus fractional BOLD change to the visual stimulus and $CO_2$ challenge for each subject in the visual ROI only. (B) Mean and standard deviation of $\delta$BOLD and $\delta$CBF to visual stimulus experiment in normoxia/normocapnia across seventeen subjects, and mean changes to $CO_2$ challenge in the baseline state, across all subjects.
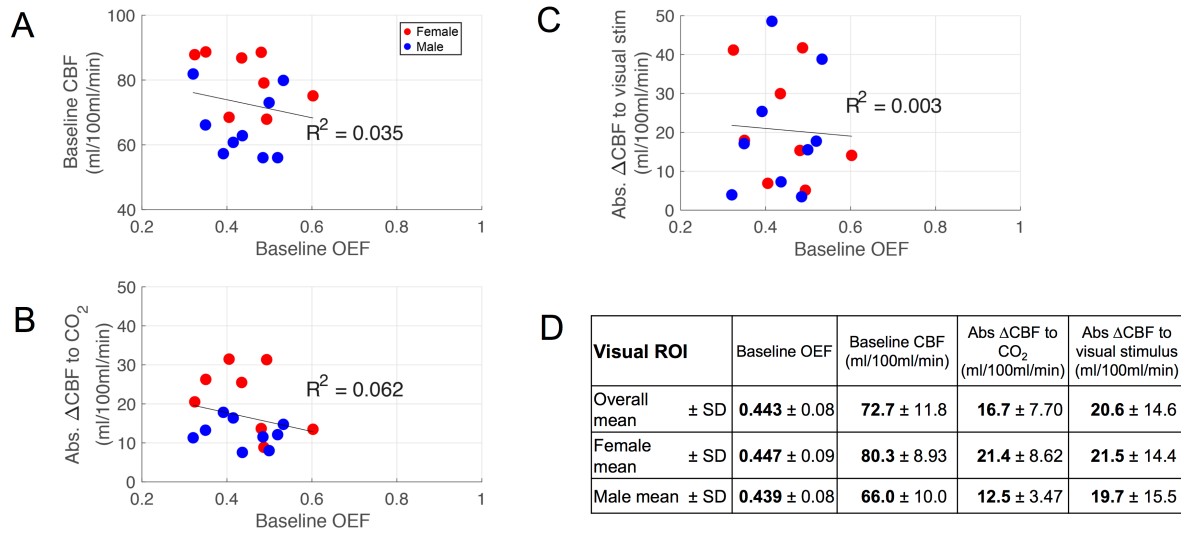
**Figure 3: VSEAN results.** (A) Independent VSEAN and ASL methods show variation of measured baseline OEF and CBF across subjects in the visually stimulated ROI. (B) Variation of OEF to absolute ΔCBF to $CO_2$ are plotted for ROI, and (C) variation across subjects versus absolute ΔCBF to visual stimulus in the visual ROI. (D) Table of baseline OEF, baseline CBF, absolute ΔCBF to $CO_2$, and absolute ΔCBF to visual stimulus in visual ROI. There was no correlation between OEF and baseline CBF or to any absolute ΔCBF. There was a significant and large effect size difference in baseline CBF between male (blue) and female (red) (p=0.007, Cohen's $d$ = 1.5).
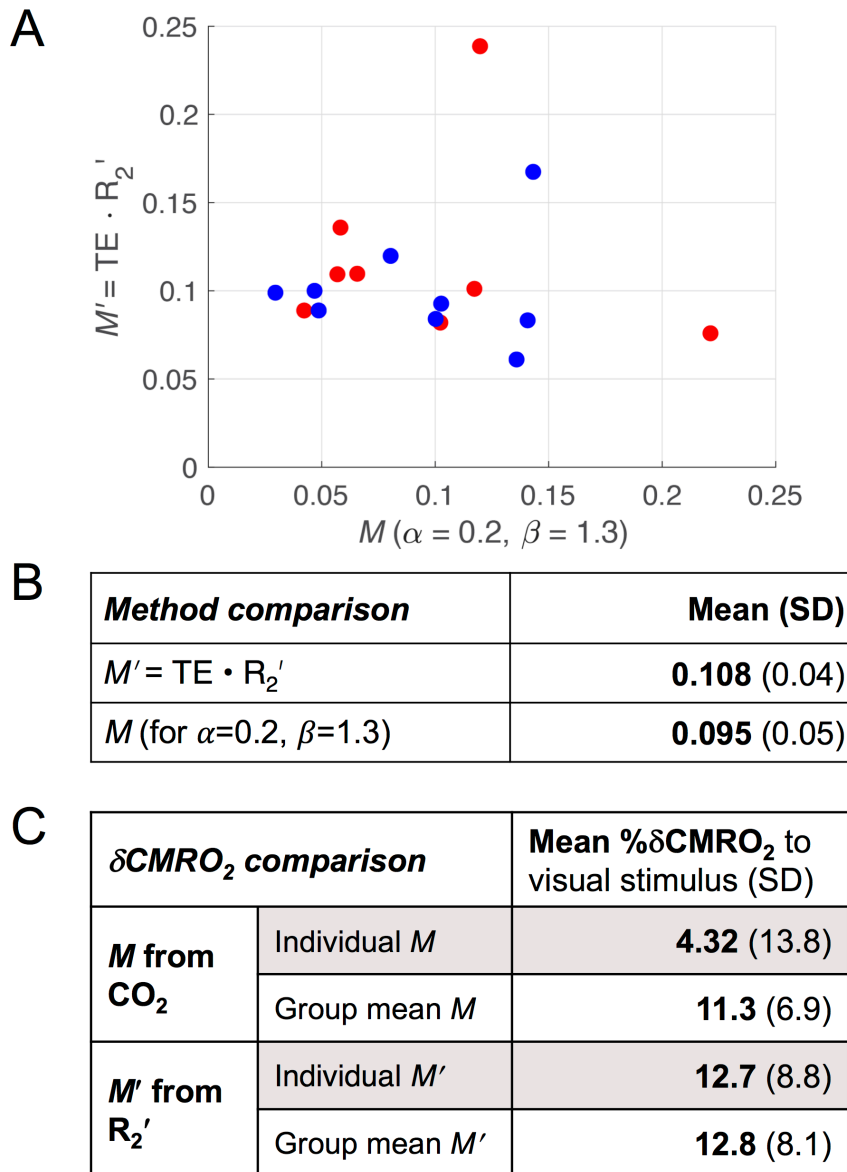
**A**

**B**

| Method comparison | Mean (SD) |
|---|---|
| $M' = TE \cdot R_2'$ | **0.108** (0.04) |
| $M$ (for $\alpha$=0.2, $\beta$=1.3) | **0.095** (0.05) |

**C**

| $\delta CMRO_2$ comparison | | Mean %$\delta CMRO_2$ to visual stimulus (SD) |
|---|---|---|
| **$M$ from CO$_2$** | Individual $M$ | **4.32** (13.8) |
| | Group mean $M$ | **11.3** (6.9) |
| **$M'$ from R$_2'$** | Individual $M'$ | **12.7** (8.8) |
| | Group mean $M'$ | **12.8** (8.1) |

**Figure 4: FLAIR-GESSE versus calibrated BOLD results.** (A) $M$ from calibrated-BOLD experiment with $\alpha$=0.2, $\beta$=1.3, and $M'$ from FLAIR-GESSE's $R_2'$ for each of 17 subjects in the visual ROI. Scatterplot demonstrates range and variance of measurements of $M$ from the two methods. (B) Average $M'$ was calculated from mean measured $R_2'$ value across 17 subjects using FLAIR-GESSE of 3.60 +/- 1.39 s$^{-1}$, with TE = 0.03 s. $M$ values were calculated from calibrated BOLD CO$_2$ experiment. (C) Fractional $\delta CMRO_2$ to visual stimulus calculated using Eq. [1] and $\delta CBF$ and $\delta BOLD$ to the visual stimulus, as well as the $M$ and $M'$ values. Two calculations were performed, one using each subject's individual $M$ or $M'$ value to calculate individual $\delta CMRO_2$, then averaged across all subjects; the other method utilized the group mean $M$ or $M'$ to calculate individual $\delta CMRO_2$, then averaged across the subjects.

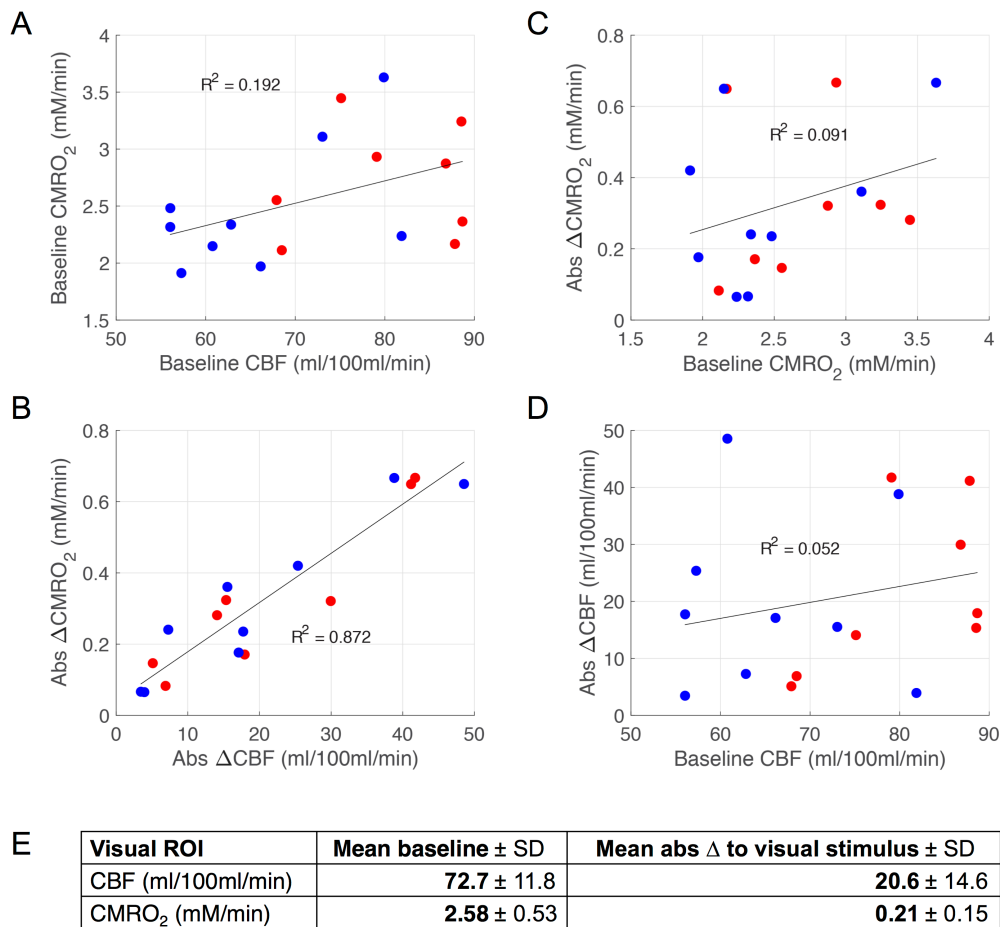| Visual ROI | Mean baseline ± SD | Mean abs Δ to visual stimulus ± SD |
|---|---|---|
| CBF (ml/100ml/min) | 72.7 ± 11.8 | 20.6 ± 14.6 |
| CMRO$_2$ (mM/min) | 2.58 ± 0.53 | 0.21 ± 0.15 |

**Figure 5: Baseline and absolute changes in CMRO$_2$ and CBF across subjects in visual ROI.** Absolute calculations of CMRO$_2$ at baseline and to a visual stimulus non-invasively determined using OEF and $M$ calibration data acquired from VSEAN and FLAIR-GESSE, with $\alpha$=0.2 and $\beta$=1.3. (A) Absolute CBF and CMRO$_2$ in the baseline state (slope=0.020, $r$=0.438, p=0.079, Cohen's $d$ = 0.97). (B) Absolute CBF and CMRO$_2$ changes in response to the visual stimulus (slope=0.014, $r$=0.934, $p$<0.00001, $d$ = 5.23). Note that x- and y-axes are not independent in A or B as CMRO$_2$ estimates are calculated from CBF. (C) Absolute ΔCMRO$_2$ change to visual stimulus versus baseline CMRO$_2$. Change in CMRO$_2$, based on fractional change of BOLD and CBF to visual stimulus, was calculated independently of baseline CMRO$_2$, which is dependent on baseline CBF and an independent VSEAN measurement of OEF. The change in CMRO$_2$ was calculated using $M'$ from individual R$_2'$ (slope=0.091, $r$=0.302, p=0.079, $d$ = 0.0.63). (D) Absolute ΔCBF change to visual stimulus versus baseline CBF. Measurements are independent; baseline CBF was calculated based on the CSF calibration scan, while ΔCBF was estimated from ASL data with visual stimulus onset (slope=0.052, $r$=0.228, p=0.379, $d$ = 0.47). (E) Mean baseline and absolute change estimates for CMRO$_2$ and CBF.

## References

Alsop, D.C., Detre, J.A., Golay, X., Günther, M., Hendrikse, J., Hernandez-Garcia, L., Lu, H., Macintosh, B.J., Parkes, L.M., Smits, M., Van Osch, M.J.P., Wang, D.J.J., Wong, E.C., Zaharchuk, G., 2015. Recommended implementation of arterial spin-labeled Perfusion mri for clinical applications: A consensus of the ISMRM Perfusion Study group and the European consortium for ASL in dementia. Magn. Reson. Med. 73, 102–116. https://doi.org/10.1002/mrm.25197

Blockley, N.P., Griffeth, V.E.M., Simon, A.B., Dubowitz, D.J., Buxton, R.B., 2015. Calibrating the BOLD response without administering gases: Comparison of hypercapnia calibration with calibration using an asymmetric spin echo. Neuroimage 104, 423–429. https://doi.org/10.1016/j.neuroimage.2014.09.061

Blockley, N.P., Stone, A.J., 2016. Improving the specificity of R2' to the deoxyhaemoglobin content of brain tissue: Prospective correction of macroscopic magnetic field gradients. Neuroimage 135, 253–260. https://doi.org/10.1016/j.neuroimage.2016.04.013

Bolar, D.S., Rosen, B.R., Sorensen, A.G., Adalsteinsson, E., 2011. QUantitative Imaging of eXtraction of oxygen and TIssue consumption (QUIXOTIC) using venular-targeted velocity-selective spin labeling. Magn. Reson. Med. 66, 1550–1562. https://doi.org/10.1002/mrm.22946

Boynton, G.M., Engel, S.A., Glover, G.H., Heeger, D.J., 1996. Linear systems analysis of functional magnetic resonance imaging in human V1. J. Neurosci. 16, 4207–21.

Brainard, D.H., 1997. The Psychophysics Toolbox. Spat. Vis. 10, 433–436. https://doi.org/10.1163/156856897X00357

Bulte, D.P., Kelly, M., Germuska, M., Xie, J., Chappell, M. a., Okell, T.W., Bright, M.G., Jezzard, P., 2012. Quantitative measurement of cerebral physiology using respiratory-calibrated MRI. Neuroimage 60, 582–591. https://doi.org/10.1016/j.neuroimage.2011.12.017

Buxton, R.B., 2013. The physics of functional magnetic resonance imaging (fMRI). Reports Prog. Phys. 76, 096601. https://doi.org/10.1088/0034-4885/76/9/096601

Buxton, R.B., 2010. Interpreting oxygenation-based neuroimaging signals: the importance and the challenge of understanding brain oxygen metabolism. Front. Neuroenergetics 2, 1–16. https://doi.org/10.3389/fnene.2010.00008

Buxton, R.B., Griffeth, V.E.M., Simon, A.B., Moradi, F., 2014. Variability of the coupling of blood flow and oxygen metabolism responses in the brain: a problem for interpreting BOLD studies but potentially a new window on the underlying neural activity. Front. Neurosci. 8, 1–6. https://doi.org/10.3389/fnins.2014.00139

Chalela, J. a, Alsop, D.C., Gonzalez-Atavales, J.B., Maldjian, J. a, Kasner, S.E., Detre, J. a, 2000. Magnetic resonance perfusion imaging in acute ischemic stroke using continuous arterial spin labeling. Stroke. 31, 680–687. https://doi.org/10.1161/01.STR.31.3.680

Chen, J.J., Pike, G.B., 2009. BOLD-specific cerebral blood volume and blood flow changes during neuronal activation in humans. NMR Biomed. 22, 1054–1062. https://doi.org/10.1002/nbm.1411

Cox, R.W., 1996. AFNI: software for analysis and visualization of functional magnetic resonance neuroimages. Comput. Biomed. Res. 29, 162–73. https://doi.org/10.1006/cbmr.1996.0014

Crawford, A., Adesanya, A., 2010. Interpretation of Arterial Blood Gases [WWW Document]. Pocket ICU Manag. URL https://anesth.unboundmedicine.com/anesthesia/view/Pocket-ICU-Management/534207/all/Interpretation_of_Arterial_Blood_Gases#2

Davenport, H.W., 1974. The ABC of acid-base chemistry: the elements of physiological blood-gas chemistry for medical students and physicians. University of Chicago Press.

Davis, T.L., Kwong, K.K., Weisskoff, R.M., Rosen, B.R., 1998. Calibrated functional MRI: mapping the dynamics of oxidative metabolism. Proc. Natl. Acad. Sci. U. S. A. 95, 1834–1839. https://doi.org/10.1073/pnas.95.4.1834

Dickson, J.D., Ash, T.W.J., Williams, G.B., Harding, S.G., Carpenter, T.A., Menon, D.K., Ansorge, R.E., 2010. Quantitative BOLD: the effect of diffusion. J. Magn. Reson. Imaging 32, 953–961. https://doi.org/10.1002/jmri.22151

Esposito, G., Horn, J. Van, Weinberger, D.R., Berman, K.F., 1996. Gender differences in cerebral blood flow as a function of cognitive state with PET. J. Nucl. … 37, 559–64.

Fraser, M., Haldeman-Englert, C., 2017. Hemoglobin [WWW Document]. UC San Diego Heal. Libr. URL http://myhealth.ucsd.edu/RelatedItems/167,hemoglobin

Gagnon, L., Sakad i , S., Lesage, F., Musacchia, J.J., Lefebvre, J., Fang, Q., Yucel, M.A., Evans, K.C., Mandeville, E.T., Cohen-Adad, J., Polimeni, J.R., Yaseen, M.A., Lo, E.H., Greve, D.N., Buxton, R.B., Dale, A.M., Devor, A., Boas, D.A., 2015. Quantifying the Microvascular Origin of BOLD-fMRI from First Principles with Two-Photon Microscopy and an Oxygen-Sensitive Nanoprobe. J. Neurosci. 35, 3663–3675. https://doi.org/10.1523/JNEUROSCI.3555-14.2015

Gagnon, L., Sakadžić, S., Lesage, F., Pouliot, P., Dale, A.M., Devor, A., Buxton, R.B., Boas, D.A., 2016. Validation and optimization of hypercapnic-calibrated fMRI from oxygen-sensitive two-photon microscopy. Philos. Trans. R. Soc. B Biol. Sci. 371. https://doi.org/10.1098/rstb.2015.0359

Gauthier, C.J., Hoge, R.D., 2013. A generalized procedure for calibrated MRI incorporating hyperoxia and hypercapnia. Hum. Brain Mapp. 34, 1053–69. https://doi.org/10.1002/hbm.21495

Golay, X., Johanna Silvennoinen, M., Zhou, J., Clingman, C.S., Kauppinen, R.A., Pekar, J.J., Van Zij, P.C.M., 2001. Measurement of tissue oxygen extraction ratios from venous blood T2: Increased precision and validation of principle. Magn. Reson. Med. https://doi.org/10.1002/mrm.1189

Griffeth, V.E.M., Blockley, N., Simon, A.B., Buxton, R.B., 2013. A New Functional MRI Approach for Investigating Modulations of Brain Oxygen Metabolism. PLoS One 8, e68122. https://doi.org/10.1371/journal.pone.0068122

Griffeth, V.E.M., Buxton, R.B., 2011. A theoretical framework for estimating cerebral oxygen metabolism changes using the calibrated-BOLD method: Modeling the effects of blood volume distribution, hematocrit, oxygen extraction fraction, and tissue signal properties on the BOLD signal. Neuroimage 58, 198–212. https://doi.org/10.1016/j.neuroimage.2011.05.077

Guo, J., Wong, E.C., 2012. Venous oxygenation mapping using velocity-selective excitation and arterial nulling. Magn. Reson. Med. 68, 1458–1471. https://doi.org/10.1002/mrm.24145

Gur, R.E., Gur, R.C., 1990. Gender Differences in Regional Cerebral Blood Flow. Schizophr. Bull. 16, 247–254. https://doi.org/10.1093/schbul/16.2.247

He, X., Yablonskiy, D.A., 2007. Quantitative BOLD: Mapping of human cerebral deoxygenated blood volume and oxygen extraction fraction: Default state. Magn. Reson. Med. 57, 115–126. https://doi.org/10.1002/mrm.21108

Ibaraki, M., Miura, S., Shimosegawa, E., Sugawara, S., Mizuta, T., Ishikawa, A., Amano, M., 2007. Quantification of Cerebral Blood Flow and Oxygen Metabolism with 3-Dimensional PET and 15O: Validation by Comparison with 2-Dimensional PET. J. Nucl. Med. 49, 50–59. https://doi.org/10.2967/jnumed.107.044008

Ishii, K., Sasaki, M., Kitagaki, H., Sakamoto, S., Yamaji, S., Maeda, K., 1996. Regional difference in cerebral blood flow and oxidative metabolism in human cortex. J Nucl Med 37, 1086–1088.

Ito, H., Kanno, I., Kato, C., Sasaki, T., Ishii, K., Ouchi, Y., Iida, A., Okazawa, H., Hayashida, K., Tsuyuguchi, N., Ishii, K., Kuwabara, Y., Senda, M., 2004. Database of normal human cerebral blood flow, cerebral blood volume, cerebral oxygen extraction fraction and cerebral metabolic rate of oxygen measured by positron emission tomography with 15 O-labelled carbon dioxide or water, carbon monoxide and oxygen: Eur. J. Nucl. Med. Mol. Imaging 31, 635–643. https://doi.org/10.1007/s00259-003-1430-8

Jurado, R., Walker, H.K., 1969. Clinical Methods The History, Physical, and Laboratory Examinations. 3rd edition., in: Clinical Methods The History, Physical, and Laboratory Examinations. 3rd Edition. pp. 371–382. https://doi.org/10.1080/01480545.2016.1245318

Kirchner, W.K., 1958. Age differences in short-term retention of rapidly changing information. J. Exp. Psychol. 55, 352–358. https://doi.org/10.1037/h0043688

Liu, E.Y., Haist, F., Dubowitz, D.J., Buxton, R.B., 2019. Cerebral blood volume changes during the BOLD post-stimulus undershoot measured with a combined normoxia/hyperoxia method. Neuroimage 185, 154–163. https://doi.org/10.1016/j.neuroimage.2018.10.032

Liu, T.T., Behzadi, Y., Restom, K., Uludag, K., Lu, K., Buracas, G.T., Dubowitz, D.J., Buxton, R.B., 2004. Caffeine alters the temporal dynamics of the visual BOLD response. Neuroimage 23, 1402–1413. https://doi.org/10.1016/j.neuroimage.2004.07.061

Liu, T.T., Wong, E.C., 2005. A signal processing model for arterial spin labeling functional MRI. Neuroimage 24, 207–215. https://doi.org/10.1016/j.neuroimage.2004.09.047

Lu, H., Xu, F., Grgac, K., Liu, P., Qin, Q., Van Zijl, P., 2012. Calibration and validation of TRUST MRI for the estimation of cerebral blood oxygenation. Magn. Reson. Med. 67, 42–49. https://doi.org/10.1002/mrm.22970

Mark, C.I., Fisher, J.A., Pike, G.B., 2011. Improved fMRI calibration: Precisely controlled hyperoxic versus hypercapnic stimuli. Neuroimage 54, 1102–1111. https://doi.org/10.1016/j.neuroimage.2010.08.070

Merola, A., Germuska, M.A., Murphy, K., Wise, R.G., 2018. Assessing the repeatability of absolute CMRO2, OEF and haemodynamic measurements from calibrated fMRI. Neuroimage. https://doi.org/10.1016/j.neuroimage.2018.02.020

Merola, A., Murphy, K., Stone, A.J., Germuska, M.A., Griffeth, V.E.M., Blockley, N.P., Buxton, R.B., Wise, R.G., 2016. Measurement of oxygen extraction fraction (OEF): An optimized BOLD signal model for use with hypercapnic and hyperoxic calibration. Neuroimage 129, 159–174. https://doi.org/10.1016/j.neuroimage.2016.01.021

Ni, W., Christen, T., Zun, Z., Zaharchuk, G., 2015. Comparison of R2′ measurement methods in the normal brain at 3 tesla. Magn. Reson. Med. https://doi.org/10.1002/mrm.25232

Noll, D.C., Fessler, J.A., Sutton, B.P., 2005. Conjugate phase MRI reconstruction with spatially variant sample density correction. IEEE Trans. Med. Imaging 24, 325–336. https://doi.org/10.1109/TMI.2004.842452

Pelli, D.G., 1997. The VideoToolbox software for visual psychophysics: transforming numbers into movies. Spat. Vis. 10, 437–442. https://doi.org/10.1163/156856897X00366

Perthen, J.E., Lansing, A.E., Liau, J., Liu, T.T., Buxton, R.B., 2008. Caffeine-induced uncoupling of cerebral blood flow and oxygen metabolism: a calibrated BOLD fMRI study. Neuroimage 40, 237–47. https://doi.org/10.1016/j.neuroimage.2007.10.049

Raichle, M.E., MacLeod, A.M., Snyder, A.Z., Powers, W.J., Gusnard, D.A., Shulman, G.L., 2001. A default mode of brain function. Proc. Natl. Acad. Sci. U. S. A. 98, 676–82. https://doi.org/10.1073/pnas.98.2.676

Rodriguez, G., Warkentin, S., Risberg, J., Rosadini, G., 1988. Sex differences in regional cerebral blood flow. J. Cereb. Blood Flow Metab. 8, 783–789. https://doi.org/10.1038/jcbfm.1988.133

Simon, A.B., Dubowitz, D.J., Blockley, N.P., Buxton, R.B., 2016. A novel Bayesian approach to

accounting for uncertainty in fMRI-derived estimates of cerebral oxygen metabolism fluctuations. Neuroimage 129, 198–213. https://doi.org/10.1016/j.neuroimage.2016.01.001

Trudnowski, R.J., Rico, R.C., 1974. Specific gravity of blood and plasma at 4 and 37 °C. Clin. Chem.

Uhlirova, H., Kılıc, K., Tian, P., Sakadz, S., Saisan, P.A., Gagnon, L., Thunemann, M., Nizar, K., Yasseen, M.A., Jr, D.J.H., Vandenberghe, M., Djurovic, S., Andreassen, O.A., Silva, G.A., Masliah, E., Kleinfeld, D., Vinogradov, S., Buxton, R.B., Einevoll, G.T., Boas, D.A., Dale, A.M., Devor, A., Devor, A., 2016a. The roadmap for estimation of cell-type- specific neuronal activity from non- invasive measurements. Proc. R. Soc. London. Ser. B Biol. Sci. https://doi.org/10.1098/rstb.2015.0356

Uhlirova, H., Kılıç, K., Tian, P., Thunemann, M., Desjardins, M., Saisan, P.A., Sakadžić, S., Ness, T. V., Mateo, C., Cheng, Q., Weldy, K.L., Razoux, F., Vandenberghe, M., Cremonesi, J.A., Ferri, C.G.L., Nizar, K., Sridhar, V.B., Steed, T.C., Abashin, M., Fainman, Y., Masliah, E., Djurovic, S., Andreassen, O.A., Silva, G.A., Boas, D.A., Kleinfeld, D., Buxton, R.B., Einevol, G.T., Dale, A.M., Devor, A., 2016b. Cell type specificity of neurovascular coupling in cerebral cortex. Elife 5. https://doi.org/10.7554/eLife.14315

Wang, J., Qiu, M., Constable, R.T., 2005. In vivo method for correcting transmit/receive nonuniformities with phased array coils. Magn. Reson. Med. 53, 666–674. https://doi.org/10.1002/mrm.20377

Wise, R.G., Harris, A.D., Stone, A.J., Murphy, K., 2013. Measurement of OEF and absolute CMRO2: MRI-based methods using interleaved and combined hypercapnia and hyperoxia. Neuroimage 83, 135–147. https://doi.org/10.1016/j.neuroimage.2013.06.008

Wong, E.C., Buxton, R.B., Frank, L.R., 1998. Quantitative imaging of perfusion using a single subtraction (QUIPSS and QUIPSS II). Magn. Reson. Med. 39, 702–708. https://doi.org/10.1002/mrm.1910390506

Yablonskiy, D.A., 1998. Quantitation of intrinsic magnetic susceptibility-related effects in a tissue matrix. Phantom study. Magn. Reson. Med. 39, 417–428. https://doi.org/10.1002/mrm.1910390312

Yablonskiy, D.A., Haacke, E.M., 1994. Theory of NMR signal behavior in magnetically inhomogeneous tissues: The static dephasing regime. Magn. Reson. Med. 32, 749–763. https://doi.org/10.1002/mrm.1910320610

Zhao, J.M., Clingman, C.S., Närväinen, M.J., Kauppinen, R.A., Van Zijl, P.C.M., 2007. Oxygenation and hematocrit dependence of transverse relaxation rates of blood at 3T. Magn. Reson. Med. https://doi.org/10.1002/mrm.21342

**Data and code availability**

The data that support the findings of this study are available from the corresponding author, RBB, upon reasonable request. The data and code sharing adopted by the authors comply with requirements by the National Institutes of Health and by the University of California, San Diego, and comply with institutional ethics approval.